Trans Indian Inst Met (2024) 77(5):1381–1391
https://doi.org/10.1007/s12666-023-03159-x

ORIGINAL ARTICLE

Enhancement of Corrosion Resistance of $Al_2O_3 + Sm_2SrAl_2O_7$ Composite Thermal Barrier Coatings by Laser Treatment

Fredy James Joseph[1] · **Shashi Bhushan Arya**[1]

Received: 15 May 2023 / Accepted: 20 October 2023 / Published online: 15 November 2023

Abstract The rare earth aluminate $Sm_2SrAl_2O_7$ was synthesized in the laboratory through a molten salt synthesis technique at 1100 °C. A composite thermal barrier coating system on Inconel 718 substrate was developed with Al_2O_3–$Sm_2SrAl_2O_7$ composite as the top coat and NiCrAlY as the bond coat using atmospheric plasma spraying. The surface of the plasma-sprayed coatings was treated using an Nd:YAG fiber laser to seal off the open porosities and reduce surface roughness. Hot corrosion tests on the laser-modified samples were performed at 700 °C and 900 °C, in aviation and marine corrosive conditions using 50 wt.% Na_2SO_4 + 50 wt.% V_2O_5 and 90 wt.% Na_2SO_4 + 5 wt.% V_2O_5 + 5 wt.% NaCl, respectively. The laser-treated samples showed higher resistance to failure than the as-coated samples under similar conditions. The corrosion products are identified, and the mechanisms involved are discussed in detail. The effect of surface modifications on the hot corrosion resistance of the coatings is investigated.

Keywords Samarium strontium aluminate · Hot corrosion · Laser treatment · Surface modification

1 Introduction

Thermal barrier coatings (TBCs) are deployed in gas turbine components to offer thermal insulation and to protect from material degradation mechanisms at higher temperatures. Such TBC systems are subjected to high-temperature oxidation, hot corrosion, and solid particle erosion, which may lead to the failure of coatings and subsequent component failure.

The conventional TBC material yttria-stabilized zirconia (YSZ) suffers from de-stabilization issues at higher temperatures [1]. Alumina has been proven as a high-temperature coating material with better stability and chemical inertness. Also, single-layer coatings with rare earth aluminates have been studied as top coat candidates [2]. In addition, different architectures like single-layer and multi-layer coatings have been tested by various researchers. The single-layer coatings may fail to offer sufficient thermal insulation, while multi-layer coatings tend to fail from thermal mismatch issues. Composite TBCs have been proven to have a better performance at higher temperatures by a dense microstructure preventing infiltration of harmful gases and corrosive salts [3, 4]. Alumina–YSZ composite coatings have offered high resistance to oxidation at 1100 °C [5]. The Al_2O_3–$Sm_2SrAl_2O_7$ composite coatings have been proven to be resistant to high-temperature oxidation and solid particle erosion, while they undergo hot corrosion attacks at higher temperatures in aviation and marine atmospheres [6, 7].

The 'hot corrosion' refers to the severe chemical attack due to the elements like Na, S, Cl, and V, which originate from the fuels and molten ash in the operating environments. The coatings may present a porous structure with cracks after exposure to hot corrosion conditions. The resistance of a system toward hot corrosion depends on the overall chemistry, reactivity, high-temperature stability, and surface conditions of the coating. A reduction in surface roughness has offered a higher CMAS (calcium–magnesium–alumina–silicate) resistance in YSZ, $GdPO_4$, and $LaPO_4$ coatings [8]. The hot corrosion resistance of YSZ TBCs has been

✉ Shashi Bhushan Arya
sbarya@nitk.edu.in

Fredy James Joseph
fredyjamesj@gmail.com

[1] Metallurgical and Materials Engineering, National Institute of Technology, Surathkal, Karnataka 575025, India

improved by laser treatment [9]. Overall, the modification of the surface can have a significant effect on the performance of the components.

The objective of this study is to investigate the hot corrosion behavior of the laser-treated Al_2O_3–$Sm_2SrAl_2O_7$ composite TBCs under aviation and marine atmospheres. The corrosion mechanisms and the significance of surface modifications on the developed coatings are discussed in detail.

2 Materials and Methods

2.1 Development of Composite TBC Coupons

The rare earth material $Sm_2SrAl_2O_7$ (SSA) was synthesized using the molten salt technique from oxide powders Sm_2O_3, SrO, and Al_2O_3. The oxide powders in proportion were thoroughly mixed in a mortar and pestle, along with the flux (NaCl + KCl). The powder mixture was heated in a muffle furnace at a temperature of 1100 °C for about 24 h. The powder was then washed in de-ionized water to remove traces of flux constituents. The washed powder was dried in a hot air oven to obtain the final $Sm_2SrAl_2O_7$ powder.

The synthesized SSA powder was mixed with alumina powder in a 30: 70 weight ratio to obtain the required composite powder. The purity of the powders was confirmed by XRD and SEM–EDS analysis and is reported elsewhere [6]. The substrate material Inconel 718 (Ni-54.69%, Cr-17.6%, Fe-17.7%, Nb-5.26%, Mo-2.83%, Al-0.22%, Ti-0.9%, Co-0.36%, Mn-0.24%) of 10 mm × 10 mm × 5 mm dimensions was cleaned, grit blasted, and coated with NiCrAlY (Ni-64.8%, Cr-22.5%, Al-10.8%, Y-1.2%) bond coat before the application of top coat. The coatings were prepared using atmospheric plasma spraying employing a mass flow-controlled plasma system AP-2700 attached with an MF4 spray gun. Argon and hydrogen were used as primary and secondary gases in the spraying process.

The surface of the atmospheric plasma-sprayed samples was treated with an Nd: YAG fiber laser to obtain better surface properties. The optimized parameters 40W power at 0.5 m/min scan speed, with a beam diameter of 500 µm, was used to scan the coated surface.

2.2 Hot Corrosion Tests

The hot corrosion behavior of the developed coatings was investigated in two conditions: aviation and marine conditions. The aviation conditions were replicated using a salt combination of 50 wt.% Na_2SO_4 + 50 wt.% V_2O_5, while the marine environment consisted of a salt combination of 90 wt.% Na_2SO_4 + 5 wt.% V_2O_5 + 5 wt.% NaCl. The corrosive slurry was prepared by mixing the constituent powders in proportion and blending with the addition of de-ionized water. The test coupons were cleaned and weighed before the application of the corrosive salts. The slurry was applied uniformly using a hair brush, with a density of 18–20 mg/cm^2 on the surface, as shown in Fig. 1. The samples were then loaded in the furnace and heated to 700 °C and 900 °C. The sample condition was visually inspected intermittently (10-h intervals) to check the failure of coatings. Any samples with major spallation of coatings were removed from the furnace. The time for failure for each samples was noted, and the photographs are taken for analysis. The developed coatings and the coating after hot corrosion tests were characterized in detail using XRD, SEM, EBSD, and Raman spectroscopy.

3 Results and Discussion

3.1 Characterization of Laser-Treated Samples

The developed composite top coat surfaces (70 wt.% Al_2O_3–30 wt.% $Sm_2SrAl_2O_7$) were treated using Nd: YAG laser, to provide a better functional surface. The laser absorption of materials is a complex phenomenon depending on both material properties and surface conditions. Different laser powers were tested on the samples to optimize the parameters.

A higher power level of 110 W showed burning of the surface. Visual inspection showed that power levels below 60 W did not cause any burning on the sample surface. Yet, the SEM observation of samples treated with 60 W displayed slight burning in a few areas, as shown in Fig. 2. The high-magnification view showed burnt marks with several pores. The microstructure observation revealed that a 40-W power at 0.5 m/min scan speed yielded a better surface with minimum roughness with no burnt marks.

The laser-treated samples showed a slightly fainted appearance than the as-coated samples, as shown in Fig. 2d. The surface of the laser-treated samples viewed in SEM as

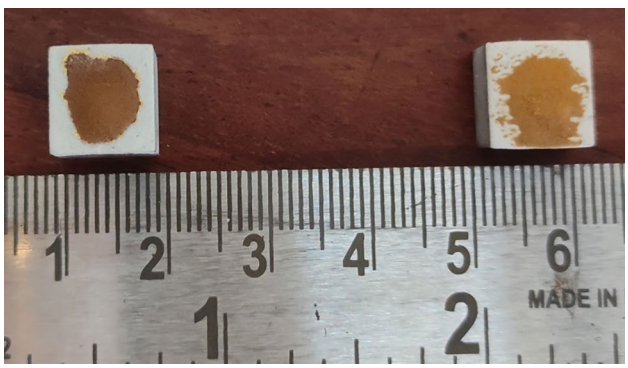

Fig. 1 The TBC samples with corrosive salts applied over the surface

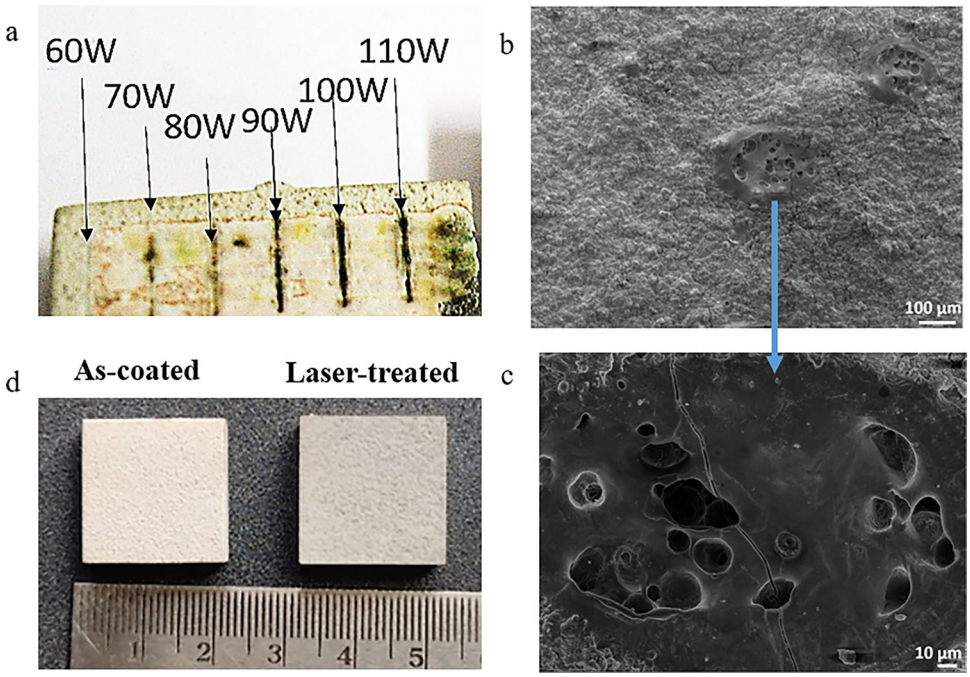

Fig. 2 **a** Optimization of laser power on developed coatings **b**, **c** low- and high-magnification views of burnt regions in samples treated with 60-W laser power, **d** photographs of as-coated and laser-treated samples

Table 1 EDS composition of laser-treated surface (wt.%)

Elements	Sm	Sr	Al	O
Laser-treated surface	17.2	4.4	39.5	38.9
As-coated surface	17.5	4.9	39.3	38.0

in Fig. 2b, c, showed a remelted surface with lower protrusions and asperities. Disc-like splats and unmolten particles were visible in the as-coated morphology. A major portion of the surface protrusions and unmolten particles have been remelted, forming a smooth surface. Similar remelted surfaces with the least discontinuities have been reported in other research [10]. Localized melting of surface asperities and solidified melt pools were visible on the laser-treated surface. Very fine microcracks have been induced during remelting, while the majority of the open porosities were sealed off. A notably higher number of open porosities were present on the as-coated surface, while the treated surface was free of pores. The laser glazing of LZ/YSZ developed holes on surfaces upon solidification, where gases in the melt pool had not enough time to escape resulting in bubble formation [11]. As only a shallow layer was being remelted, the cooling did not produce any shrinkage porosities, as observed in microstructure analysis. The presence of shrinkage porosities generally leads to a weakened material by gas entrapment and discontinuities [12].

The EDS analysis was carried out on the treated surface to monitor any changes in composition that occurred during the laser exposure. No noticeable difference in composition was detected after laser treatment (Table 1).

The non-contact profilometric analysis of the laser-treated surface using a Nanovea ST-400 surface profilometer, as shown in Fig. 3b, measured an average roughness of 4.0 µm, while the initial roughness of the as-coated samples was about 6.0 µm. The profilometric view showed peaks and valleys of lower magnitude, while the line scan measured a lower amplitude of roughness peaks. A lower and upper cutoff values of 2.5 µm and 0.8 mm were followed for roughness measurements. Similar instances of reduced roughness achieved in plasma-sprayed YSZ coatings through laser treatment have been reported [13].

The XRD pattern of the laser-treated surface is shown in Fig. 4a. The fraction of the phases present remained the same as that of as-coated systems with 30% of $Sm_2SrAl_2O_7$, 53.8% of Υ-Al_2O_3, and 16.7% of α-Al_2O_3 (JCPDS Card No 01-074-3404, 00-029-0063, and 00-042-1468, respectively). The laser glazing did not influence the phase formation in the considered system. Cases of α-Al_2O_3 formation upon laser treatment of Υ-Al_2O_3 have been reported, which is not observed in the present study [14]. The variation in behavior may be due to the difference in material composition and surface conditions. Intensity variations in the peaks have been identified, in reflection of the microstructural variations after remelting [13–15]. Researchers suggest that laser treatment can make significant changes in the orientation of planes within the system [16].

The EBSD analysis was carried out on laser-treated samples after thorough cleaning using acetone. No surface preparation techniques were employed on the samples to monitor any deviations from the plasma-sprayed condition upon laser treatment. The EBSD phase map of the laser-treated

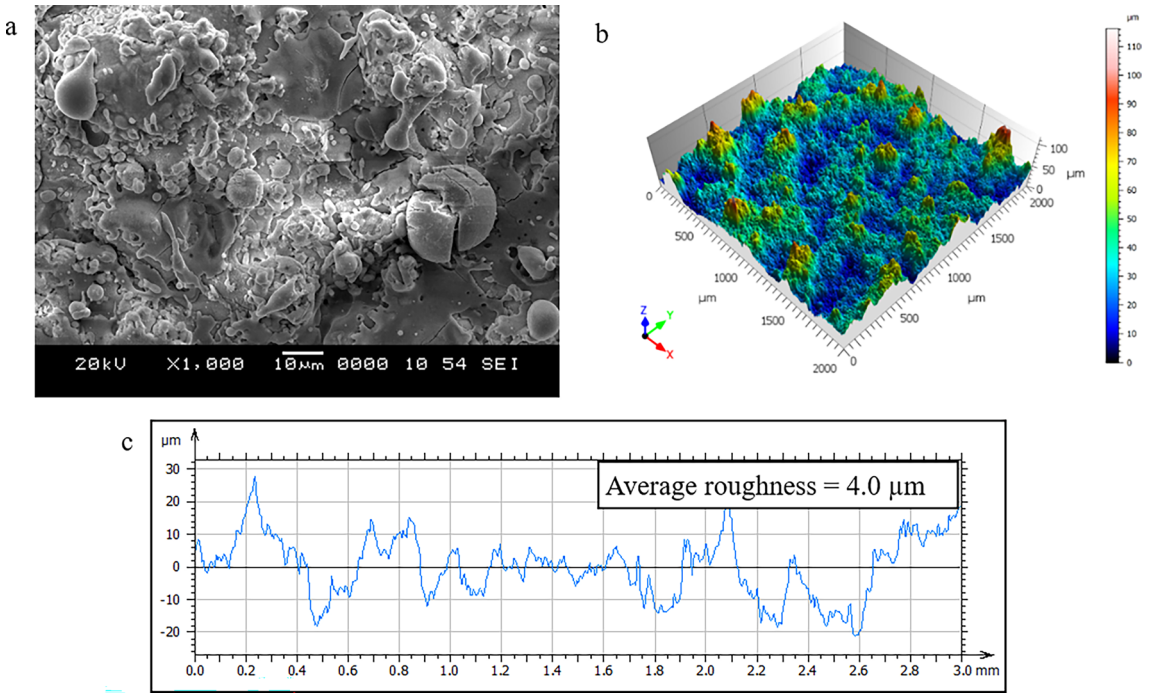

Fig. 3 **a** Surface morphology, **b** profilometric view, and **c** surface roughness profile of laser-treated sample surface

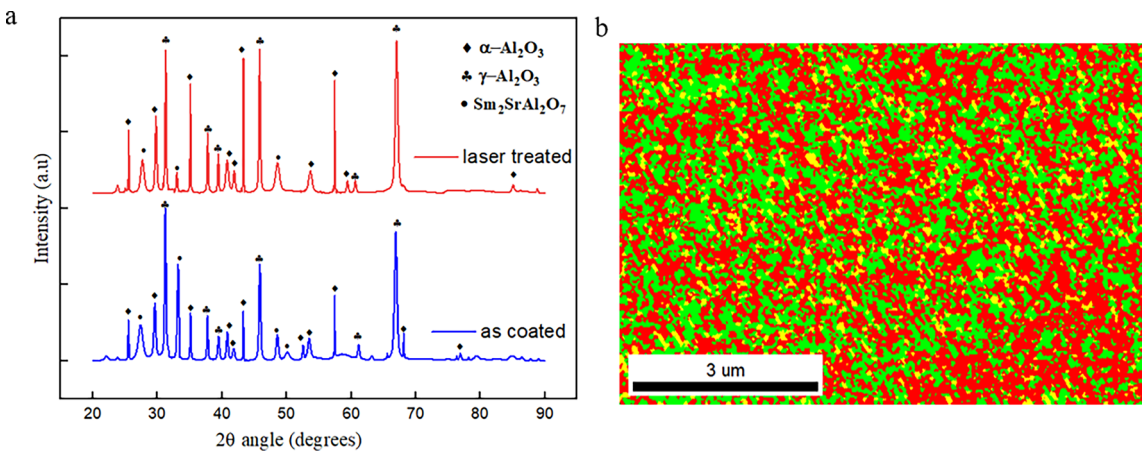

Fig. 4 **a** Surface XRD pattern of as-coated and laser-treated samples, **b** EBSD phase mapping of the laser-treated samples

surface confirmed the distribution of the phases as found by the XRD analysis. The phase distribution was found to be uniform, with a very fine grain size. Also, no segregation of phases was observed in the system after laser treatment.

3.2 Mechanical Properties of Laser-Treated Samples

Nanoindentation measurements have been taken on the samples using a Berkovich diamond indenter of 20-nm tip, as shown in Fig. 5. An average hardness of 12.6 GPa and an increased Young's modulus of 176 GPa were obtained in the laser-treated samples (Table 2). Multiple measurements were taken, and the average value is presented. The observed hardness was 8.7% higher than that of as-coated samples due to the remelting and solidification during laser exposure. A higher improvement in hardness was not obtained, as the alumina phase fractions remained the same after the laser treatment. The alpha phase of alumina being denser, the retention of the alpha phase could have offered a better enhancement in hardness. The melting of protrusions and closure of surface pores were solely responsible for the variation in hardness. The nearly 15% increase in Young's

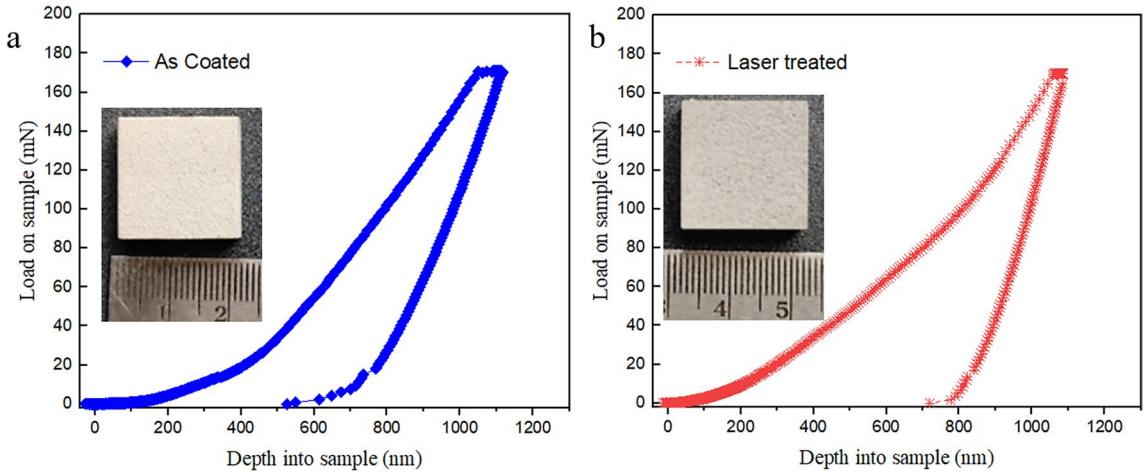

Fig. 5 Nanoindentation profiles of as-coated and laser-treated samples

Table 2 Mechanical properties of as-coated and laser-treated samples

	Young's modulus (GPa)	Hardness (GPa)
As-coated	152	11.5
Laser-treated	176	12.6

modulus reflects the sintering of the composite coatings during laser treatment.

3.3 Hot Corrosion Behavior of Laser-Treated TBCs

Figure 6a shows the resistance of laser-treated TBCs in different corrosive salt conditions. At 700 °C, the coatings exposed to marine conditions showed a 16.1% lower resistance than the samples exposed to aviation conditions. Similarly, at 900 °C, a 13% lower resistance was realized for samples in marine atmospheres. The photographs of the laser-treated samples after the hot corrosion test are shown

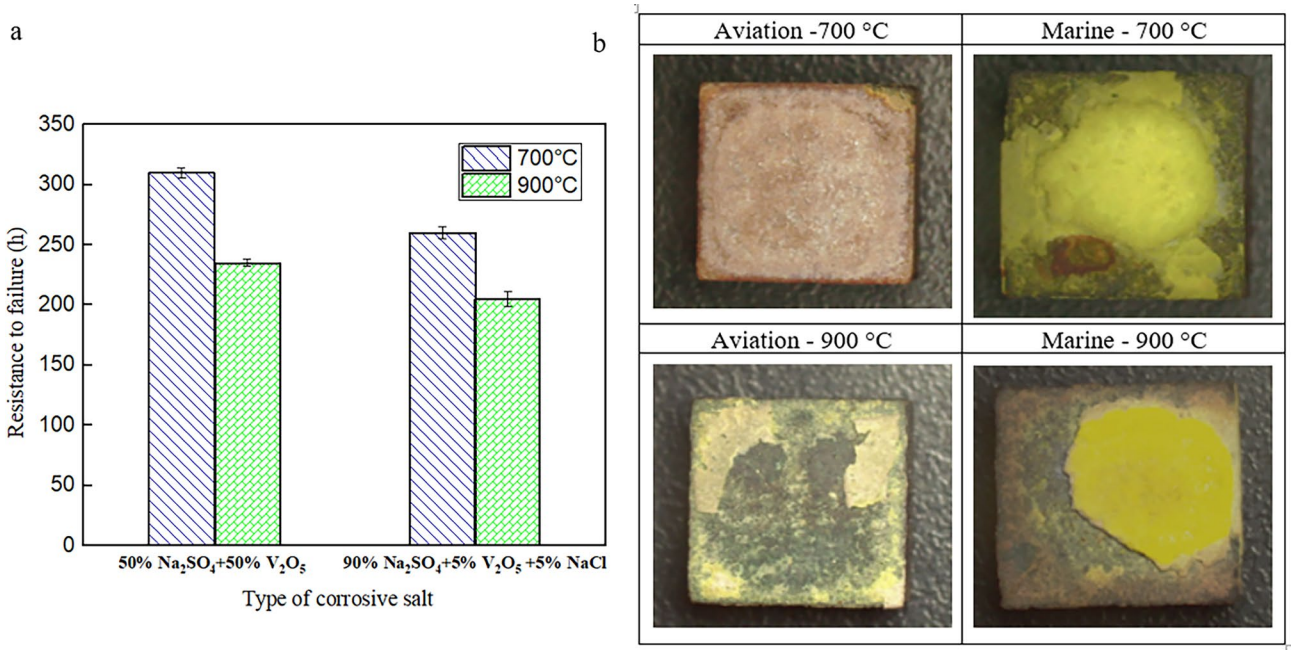

Fig. 6 **a** Hot corrosion resistances of laser-treated samples and **b** photographs of laser-treated samples in different corrosive conditions

in Fig. 6b. In most of the conditions, coatings have been chipped off in a major surface area. A similar failure mode was reported in the case of plasma-sprayed SSA-Al_2O_3 composite coatings under similar environments [7].

3.4 Hot corrosion in Aviation Environments at 700 °C and 900 °C

The XRD pattern of the laser-treated sample exposed to aviation conditions at 700 °C is shown in Fig. 7a. The peaks corresponding to corrosion products $SmAlO_3$ (JCPDS Card No 00-029-0083), $SmVO_4$ (JCPDS Card No 00-017-0876), $AlVO_4$ (JCPDS Card No 00-039-0276), $SrAl_2O_4$ (JCPDS Card No 00-034-0379), and $NaAlO_2$ (JCPDS Card No 00-033-1200) have been identified on the surface of the coating. The $SmAlO_3$ formed from the decomposition of the top coat showcased the dominating peak in the pattern. It is worth mentioning that, the material composition being the same, the products evolved were identical to that in the case of as-coated samples. The microstructure examination showed rod-like structures developed on the surface (Fig. 7b, c) identified as $SmVO_4$ (Table 3). In the case of as-coated samples in the same atmosphere, needle-like structures of $SmVO_4$ were identified instead of rods.

The XRD pattern of the laser-treated sample exposed to aviation conditions at 900 °C is shown in Fig. 8. The corrosion products $SmAlO_3$, $SmVO_4$, $AlVO_4$, $SrAl_2O_4$, and $NaAlO_2$ have been identified, with the $SmVO_4$ peak showing

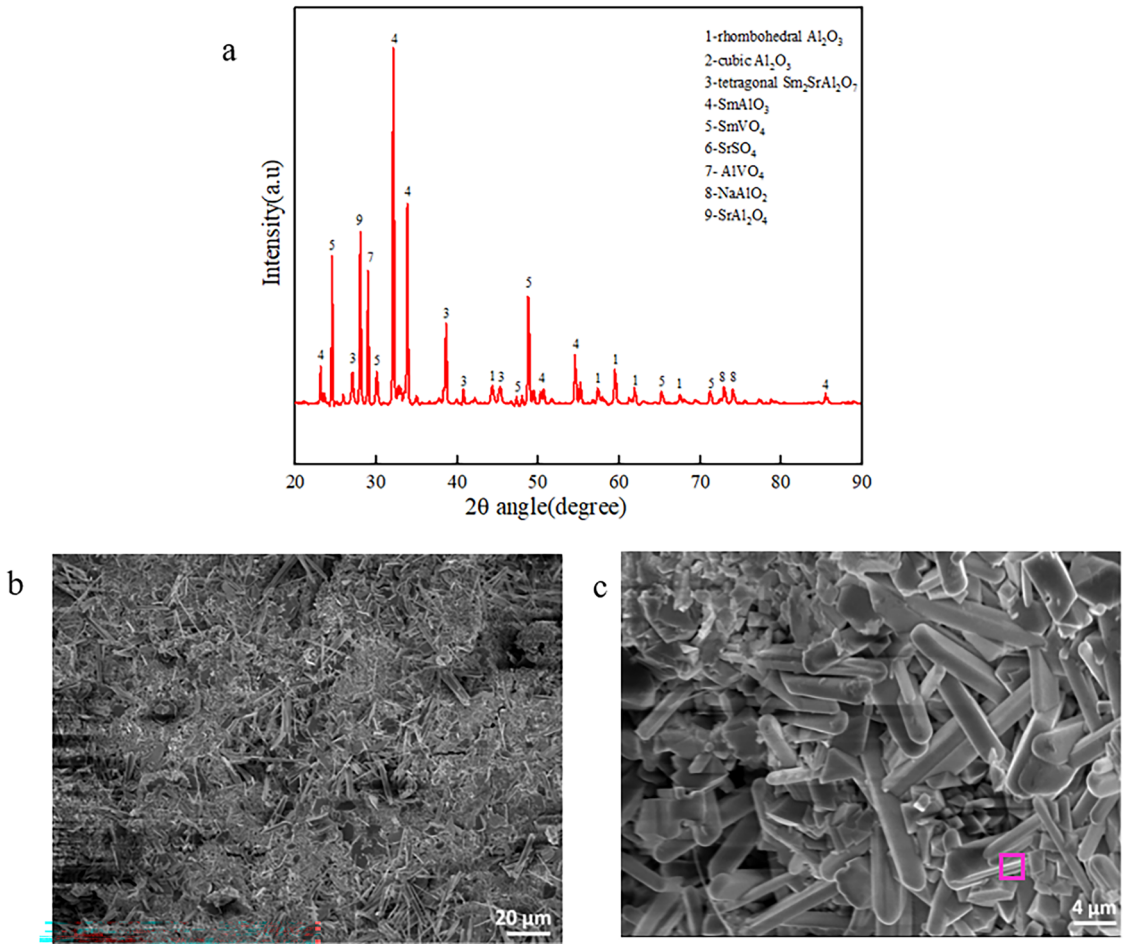

Fig. 7 **a** XRD pattern, **b**, **c** low- and high-magnification SEM images of laser-treated samples exposed to aviation hot corrosion conditions at 700 °C

Table 3 Composition of the products (wt.%) formed on laser-treated samples exposed to aviation conditions

Element	Sm	Sr	Al	O	Na	S	V
700 °C	57.1	0.00	0.00	23.80	0.00	0.00	19.00
900 °C	56.08	0.00	0.00	23.71	0.00	0.00	20.23

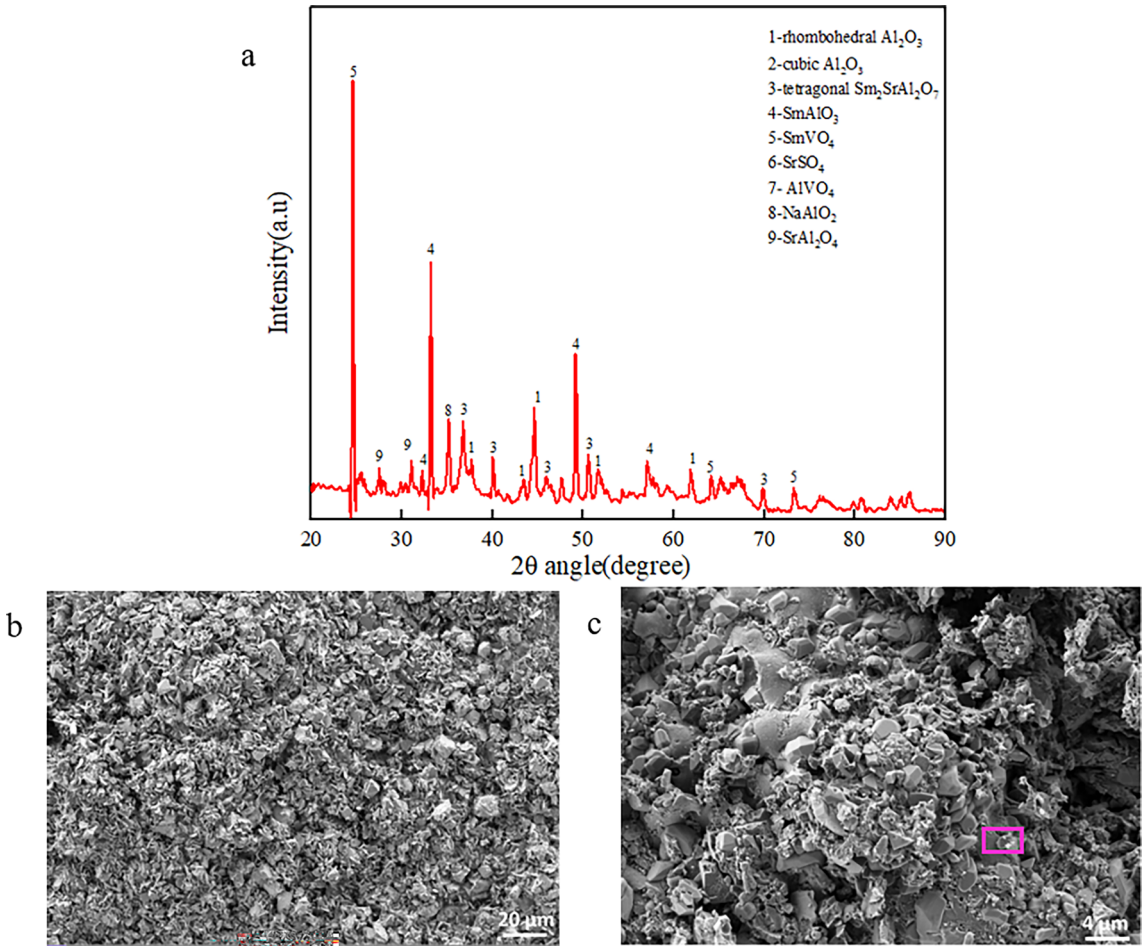

Fig. 8 **a** XRD pattern, **b**, **c** low- and high-magnification SEM images of laser-treated samples exposed to aviation hot corrosion conditions at 900 °C

the highest intensity. Under these conditions, the primary product $SmVO_4$ was common in both as-coated and laser-treated samples. The laser samples contained $NaAlO_2$ and $SrAl_2O_4$, which was not found in the as-coated sample.

The high-magnification images of the corroded surface (Fig. 8c) showed cuboidal structures of $SmVO_4$, with the composition listed in Table 3. The as-coated samples in the same environment presented cuboidal and pyramidal structures with a larger size than in laser-treated samples. As in Fig. 9, Raman spectroscopy of the corroded surfaces was examined to confirm the products formed. In the spectrum, the high-intensity peak of $SmVO_4$ at 877 cm^{-1} (O–Sm–O) and 814 cm^{-1} (Sm–O) was visible, in agreement with the XRD patterns [17].

3.5 Hot corrosion in Marine Environment at 700 °C and 900 °C

The XRD pattern of the laser-treated samples exposed to marine conditions (90% wt. Na_2SO_4 + 5%wt. V_2O_5 + 5%wt.

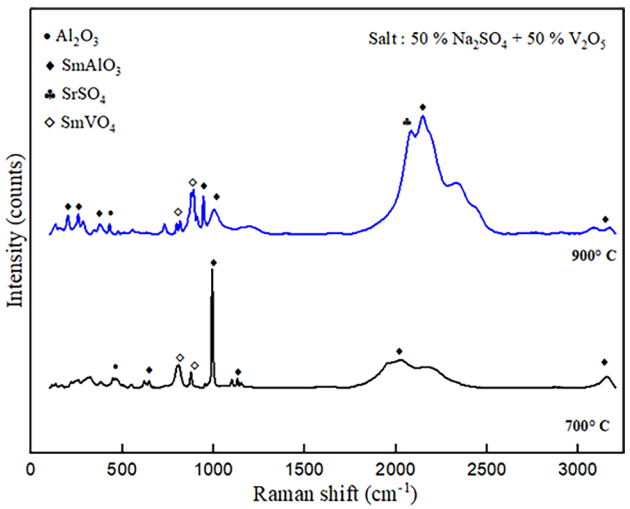

Fig. 9 Raman spectrum of laser-treated samples after hot corrosion in aviation conditions at 700 °C and 900 °C

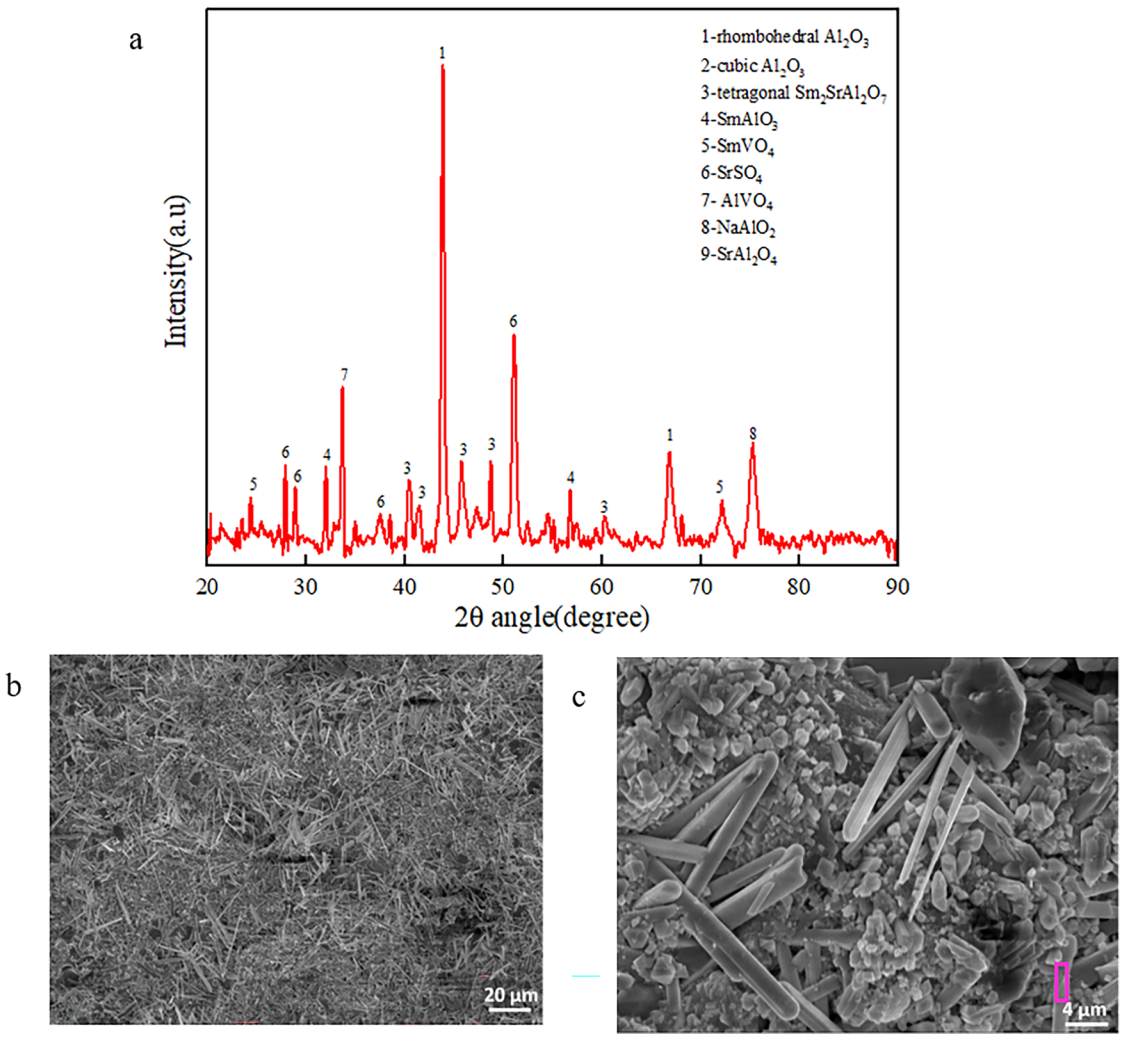

Fig. 10 **a** XRD pattern, **b**, **c** low- and high-magnification SEM images of laser-treated samples exposed to marine hot corrosion conditions at 700 °C

NaCl) at 700 °C is shown in Fig. 10a. The pattern showed peaks corresponding to Al_2O_3, SSA, $SmAlO_3$, $SmVO_4$, $AlVO_4$, $NaAlO_2$, and $SrSO_4$ (JCPDS Card No 00–005-0593). The compounds $SrSO_4$ and $AlVO_4$ presented higher intensities than the rest. In this case, the higher sulfate content may have led to the formation of $SrSO_4$. The high-magnification images showcased a mixture of rods and smaller cuboidal-shaped $SrSO_4$ (Fig. 10b, c). Table 4 shows the composition of the corrosion products measured by EDS in the labeled regions.

The XRD pattern of the laser-treated samples after hot corrosion in marine conditions at 900 °C is shown in Fig. 11a. Besides the top coat peaks, corrosion-evolved $SmAlO_3$, $SmVO_4$, $NaAlO_2$, and $SrSO_4$ were detected. The dissociation component $SmAlO_3$ dominated the peak intensity. The high-magnification SEM images showed a more damaged surface in the chloride environment. Rod-like and block-like $SrSO_4$ have been identified in the microstructure as shown in Fig. 11b, c. The Raman spectrum of the laser-treated samples after hot corrosion is shown in Fig. 12. The presence of $SrSO_4$ peaks at

Table 4 Composition of the products (wt.%) formed on laser-treated samples exposed to marine conditions

Element	Sm	Sr	Al	O	Na	S	V	Cl
700 °C	0.00	47.93	0.00	35.06	0.00	17.00	0.00	0.00
900 °C	0.00	47.33	0.00	34.37	0.00	18.26	0.00	0.00

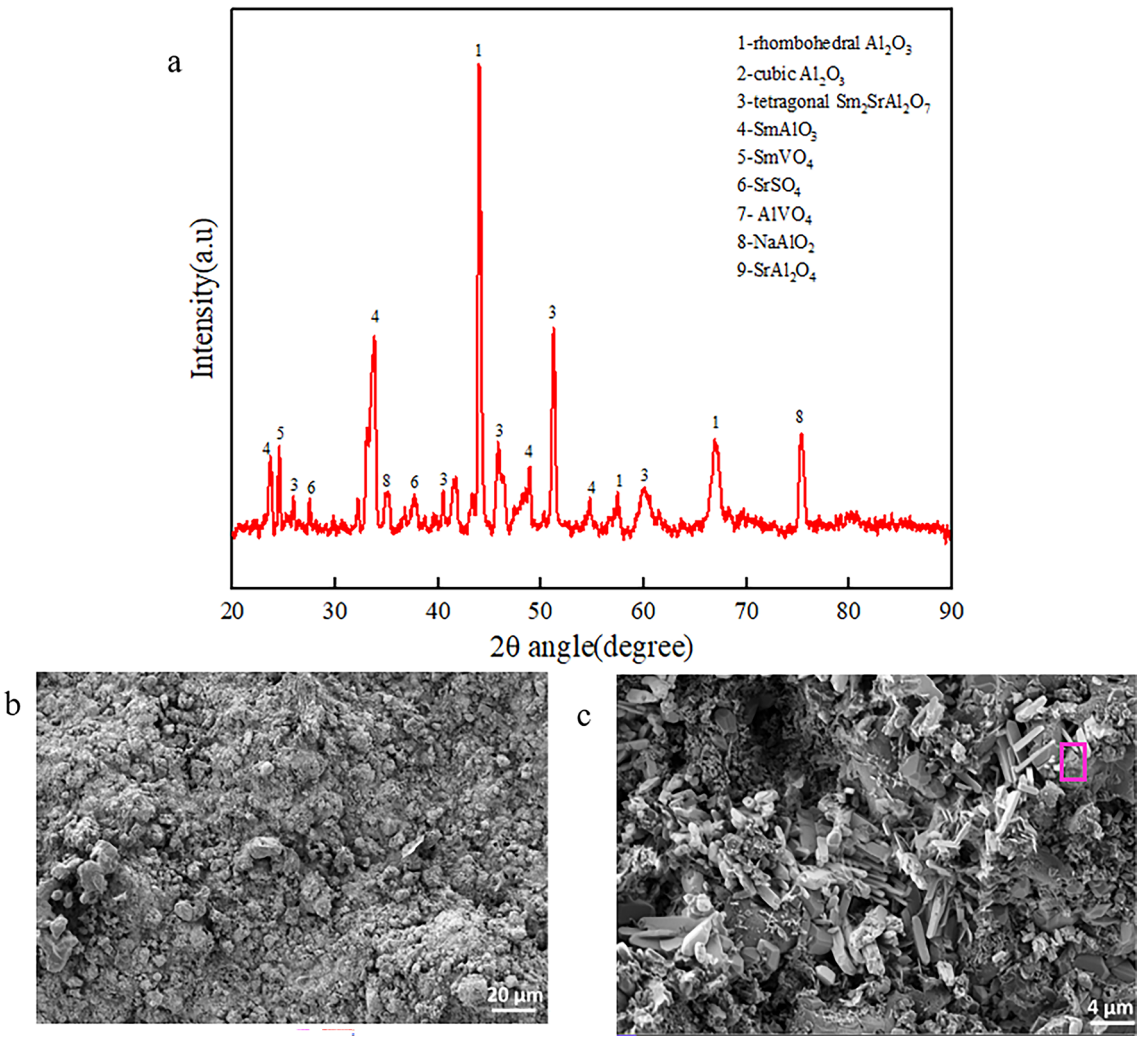

Fig. 11 **a** XRD pattern, **b**, **c** low- and high-magnification SEM images of laser-treated samples exposed to marine hot corrosion conditions at 900 °C

1001 cm^{-1} was confirmed in agreement with EDS and XRD observations [18].

3.6 Overview of Corrosion Interactions

On investigating the laser-treated composite TBCs exposed to hot corrosion, it can be inferred that the composite is prone to failure in the presence of corrosive salts. Upon corrosion, $Sm_2SrAl_2O_7$ dissociates into less stable compounds, which react further with the sulfates and vanadates. The dissociation product $SmAlO_3$ is found in every sample, irrespective of the prevailing corrosion conditions.

From the XRD and EDS analysis, the composite dissociation is assumed to be as follows.

$$Sm_2SrAl_2O_7 + Al_2O_3 \rightarrow 2SmAlO_3 + SrAl_2O_4 \quad (1)$$

$SmAlO_3$ can also form from the decomposition of $Sm_2SrAl_2O_7$ to $SmAlO_3$ and SrO as

$$Sm_2SrAl_2O_7 \rightarrow 2SmAlO_3 + SrO \quad (2)$$

The possible mechanism of the formation of $SmVO_4$ in aviation conditions is given as:

$$Na_2SO_4 + V_2O_5 \rightarrow 2NaVO_3 + SO_3 \quad (3)$$

$$Sm_2O_3 + 2NaVO_3 \rightarrow 2SmVO_4 + Na_2O \quad (4)$$

The significance of the corrosion mixture selected is the formation of $NaVO_3$ and their congruent melting around 610 °C [19]. The presence of $NaVO_3$ is not generally desired in the environment. The $NaVO_3$ formation in a conventional YSZ TBC system has been reported to

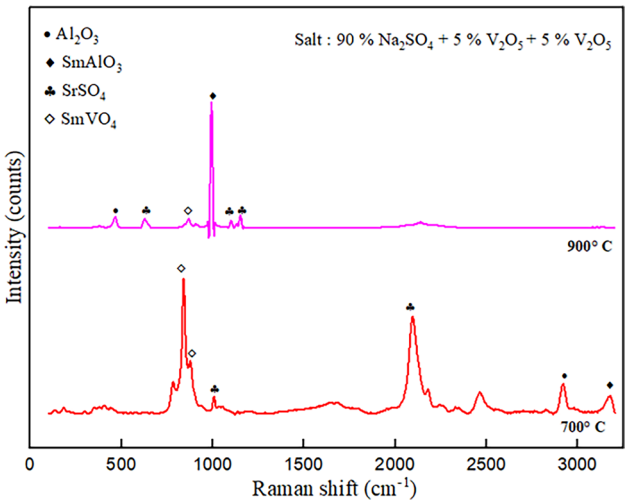

Fig. 12 Raman spectrum of laser-treated samples after hot corrosion in marine conditions at 700 °C and 900 °C

accelerate the depletion of yttria from YSZ, by increasing the atomic mobility, causing coating failure.

In marine conditions, the $SrAl_2O_4$ formed reacts with Na_2SO_4 to form $SrSO_4$ and $2NaAlO_2$.

$$SrAl_2O_4 + Na_2SO_4 \rightarrow SrSO_4 + 2NaAlO_2 \quad (5)$$

$$Na_2SO_4 \rightarrow Na_2O + SO_3 \quad (6)$$

$$Al_2O_3 + Na_2O \rightarrow 2NaAlO_2 \quad (7)$$

The decomposition of Na_2SO_4 results in the formation of Na_2O and SO_3, in which Na_2O reacts with Al_2O_3 to form $NaAlO_2$, which aids in slowing down further hot corrosion of alumina [16, 17].

Interestingly, the dominance of gamma alumina was not observed in any samples after hot corrosion. Alpha alumina is highly inert to chemical interactions than gamma alumina. The porous gamma alumina possesses a high surface area, which tends to increase the reactivity. The reactivity of solid reactants increases with an increase in surface area. Besides, the alpha alumina bulk shows higher stability than the gamma alumina bulk [18–21]. The Υ-Al_2O_3 reacted with the corrosives, while the α-Al_2O_3 offered more resistance. This sheds light on the fact that retention of the alpha phase upon thermal spraying can aid better corrosion resistance.

At 700 °C and 900 °C, $SrSO_4$ is observed to be formed only under abundance of sulfates in marine conditions. It can be inferred that the introduction of V_2O_5 into Na_2SO_4 changes the overall reaction mechanism and forms corrosive products at temperatures lower than the melting point of Na_2SO_4 [22, 23].

Table 5 Observed improvement in hot corrosion resistance after laser treatment

	Aviation conditions		Marine conditions	
	700 °C	900 °C	700 °C	900 °C
As-coated (time to failure-h)	275	215	235	190
Laser-treated (time to failure-h)	310	235	260	205
Improvement in hot corrosion resistance (%)	12.7	9.3	10.6	7.8

In all the samples, no substrate diffusion was observed, as Al_2O_3 coatings are well known for mitigating substrate migration than conventional YSZ coatings [24, 25]. Generally, the alumina layer is capable of suppressing harmful melt infiltration toward the substrate.

The corrosive attack and breakdown of protective scales are higher in the presence of chlorides, which may have led to an early failure in marine atmospheres [6, 26]. Chlorine-induced active corrosion and breakaway of dense protective films are reported to be major failure mechanisms in high-temperature components [27]. Also, the higher sulfate content in marine conditions tends to induce a de-adhesion and subsequent spallation, if it infiltrates through pores into the coating [28, 29]. It is worth mentioning that no major cracks were noticed on the corroded surface. This does not entirely eradicate the cracking possibility, as the cracks may be covered up with the corrosion products formed. In addition, no evidence of the applied corrosive salts in their original form was found pointing to the complete consumption.

3.7 An Analogy of Hot Corrosion in as-Coated and Laser-Treated Samples

Comparing the performance of as-coated and laser-treated 70 wt.% Al_2O_3—30 wt.% $Sm_2SrAl_2O_7$ coatings, the laser-treated samples showed better resistance to hot corrosion, as comprised in Table 5. At higher temperatures, the corrosive salt melt has a sufficiently low viscosity to penetrate through the open porosities and cracks on the surface of as-coated samples. The closure of porosities and sintering led to higher hot corrosion resistance in the laser-treated composite coatings by hindering the passages for infiltration. The laser treatment and subsequent reduction in roughness led to a reduced specific surface area exposed to corrosive salts. In the case of YSZ, the laser-treated samples offered a higher life with YVO_4 and m-ZrO_2 as corrosion products. In the morphology of laser-treated samples, few microcracks were present. Microcracks on laser-glazed YSZ are reported to provide an easy path for molten corrosive infiltration [8, 24]. On the other hand, if the cracks are completely removed, the glazed layer may tend to spall during operation, suffering

from a lower strain tolerance. Better resistance in the coatings can be obtained by retaining the alpha phase or by producing the alpha phase by surface treatments.

Overall, the surface modification has enhanced the hot corrosion resistance of the TBC system. Optimizing the laser treatment to eradicate any surface defect or producing the alpha phase of alumina can lead to a better hot corrosion resistance of the composite coatings.

4 Conclusions

- The laser-treated 70 wt.% Al_2O_3–30 wt.% $Sm_2SrAl_2O_7$ samples showed better hot corrosion resistance than the as-coated samples due to the sealing of open porosities through laser treatment.
- $SmVO_4$ and $SrSO_4$ were the major corrosion products observed in aviation and marine conditions, respectively.
- The samples were least resistant to hot corrosion in marine conditions than in aviation conditions.

Acknowledgements The authors would like to thank the Metallizing Equipments, Jodhpur, and RRCAT, Indore, for the support offered in the development of samples. The authors are also thankful to CRF NITK for providing the characterization facilities. The help received from the operators Mr. Akash, Mrs. Aniz, Mr. Sanath, and Mr. Pradeep is greatly acknowledged.

Funding The authors did not receive support from any organization for the submitted work.

Declarations

Conflict of interest The authors have no financial or proprietary interests in any material discussed in this article.

References

1. Bajpai P, Das A, Bhattacharya P, Madayi S, Kulkarni K, and Omar S, *J. Am. Ceram. Soc.* **98** (2015) 2655. https://doi.org/10.1111/jace.13631
2. Baskaran T, and Arya S B, *Ceram. Int.* (2018). https://doi.org/10.1016/j.ceramint.2018.06.234
3. Avci A, Eker A A, and Karabas M, *Int. J. Mater. Res.* **111** (2020) 1.
4. Karabaş M, Bal E, and Taptik Y, *Protection of Metals and Physical Chemistry of Surfaces* **53** (2017) 859. https://doi.org/10.1134/S2070205117050069
5. Keyvani A, Saremi M, Heydarzadeh Sohi M, Valefi Z, Yeganeh M, and Kobayashi A, *J. Alloys Compd.* **600** (2014) 158. https://doi.org/10.1016/j.jallcom.2014.02.004
6. James Joseph F, Arya S B, and Satish Kumar D, *Mater. Corros.* (2023). https://doi.org/10.1002/maco.202313813
7. Joseph F J, Arya S B, and Tailor S, *Mater. Corros.* **5** (2022) 1. https://doi.org/10.1002/maco.202213401
8. Guo L, Li G, and Gan Z, *J. Adv. Ceram.* **10** (2021) 472. https://doi.org/10.1007/s40145-020-0449-7
9. Guo L, Xin H, Zhang Z, Zhang X, and Ye F, *J. Adv. Ceram.* **9** (2020) 232. https://doi.org/10.1007/s40145-020-0363-z
10. Wang D, Tian Z, Shen L, Liu Z, and Huang Y, *Ceram. Int.* **40** (2014) 8791. https://doi.org/10.1016/j.ceramint.2014.01.101
11. Arshad A, Yajid M A M, and Idris M H, *Mater. Today Proc.* **39** (2021) 941. https://doi.org/10.1016/j.matpr.2020.04.145
12. Zhang Z, Tan X H, Zhang J, and Shan J G, *Int. J. Adhes. Adhes.* **85** (2018) 184. https://doi.org/10.1016/j.ijadhadh.2018.06.013
13. Múnez C J, Gómez-García J, Sevillano F, Poza P, and Utrilla M V, *J. Nanosci. Nanotechnol.* **11** (2011) 8724. https://doi.org/10.1166/jnn.2011.3457
14. Moriya R, Iguchi M, Sasaki S, and Yan J, *Procedia CIRP* **42** (2016) 464. https://doi.org/10.1016/j.procir.2016.02.233
15. Ghasemi R, Shoja-Razavi R, Mozafarinia R, and Jamali H, *Ceram. Int.* **40** (2014) 347. https://doi.org/10.1016/j.ceramint.2013.06.008
16. Tsai P C, Lee J H, and Chang C L, *Surf. Coatings Technol.* **202** (2007) 719. https://doi.org/10.1016/j.surfcoat.2007.07.005
17. Govindarajan G, Joy Johanson F, Uma Shankar V, and Joseph Salethraj M, *Mater. Technol.* (2021). https://doi.org/10.1080/10667857.2021.1985750
18. Chen Y H, Huang E, and Yu S C, *Solid State Commun.* **149** (2009) 2050. https://doi.org/10.1016/j.ssc.2009.08.023
19. Jana P, Jayan P S, Mandal S, and Biswas K, *Surf. Coat. Technol.* **322** (2017) 108. https://doi.org/10.1016/j.surfcoat.2017.05.038
20. Afrasiabi A, Saremi M, and Kobayashi A, *Mater. Sci. Eng. A* **478** (2008) 264. https://doi.org/10.1016/j.msea.2007.06.001
21. Baskaran T, Synthesis and development of $Sm_2SrAl_2O_7$ based air plasma sprayed ceramic thermal barrier coatings: oxidation, hot corrosion and high temperature erosion study (2018).
22. Busca G, *Catal. Today* **226** (2014) 2. https://doi.org/10.1016/j.cattod.2013.08.003
23. Yugeswaran S, Kobayashi A, and Ananthapadmanabhan P V, *J. Eur. Ceram. Soc.* **32** (2012) 823. https://doi.org/10.1016/j.jeurceramsoc.2011.10.049
24. Ramaswamy P, Seetharamu S, and Raob K J, *Compos. Sci. Technol.* **57** (1997) 81.
25. Gurrappa I, *Oxid. Met.* **51** (1999) 353. https://doi.org/10.1023/a:1018831025272
26. Andersson J M, *Controlling the Formation and Stability of Alumina Phases*, Linköping University, Linköping (2005).
27. Sadeghi E, Markocsan N, and Joshi S, *Advances in Corrosion-Resistant Thermal Spray Coatings for Renewable Energy Power Plants. Part I: Effect of Composition and Microstructure*, vol. 28. Springer, Berlin (2019).
28. Jarvis E, and Carter E, *Comput Sci. Eng.* **1** (2002) 33.
29. Reza M S, Aqida S N, and Ismail I, *IOP Conference Series: Materials Science and Engineering* (2018). https://doi.org/10.1088/1757-899X/319/1/012067